

Constraints on the braneworld from compact stars

R. González Felipe^{a,b} D. Manreza Paret,^c and A. Pérez Martínez^d

^aISEL - Instituto Superior de Engenharia de Lisboa, Instituto Politécnico de Lisboa,
Rua Conselheiro Emídio Navarro 1959-007 Lisboa, Portugal

^bDepartamento de Física and Centro de Física Teórica de Partículas - CFTP, Instituto
Superior Técnico, Universidade de Lisboa, Avenida Rovisco Pais, 1049-001 Lisboa, Portugal

^cDepartamento de Física General, Facultad de Física, Universidad de la Habana, La Habana,
10400, Cuba

^dInstituto de Cibernética, Matemática y Física (ICIMAF), La Habana, 10400, Cuba

E-mail: ricardo.felipe@tecnico.ulisboa.pt, dmanreza@fisica.uh.cu,
aurora@icimaf.cu

Abstract. According to the braneworld idea, ordinary matter is confined on a 3-dimensional space (brane) that is embedded in a higher-dimensional space-time where gravity propagates. In this work, after reviewing the limits coming from general relativity, finiteness of pressure and causality on the brane, we derive observational constraints on the braneworld parameters from the existence of stable compact stars. The analysis is carried out by solving numerically the brane-modified Tolman-Oppenheimer-Volkoff equations, using different representative equations of state to describe matter in the star interior. The cases of normal dense matter, pure quark matter and hybrid matter are considered.

Contents

1	Introduction	1
2	TOV equations on the brane	3
3	Compactness limits in the braneworld	5
4	Brane TOV solutions and observational constraints	9
4.1	Pure neutron stars with nucleon-nucleon interactions	10
4.2	Quark stars	11
4.3	Hybrid stars	14
5	Conclusions	16

1 Introduction

Braneworld ideas and, particularly, the Randall-Sundrum (RS) models [1, 2], have been extensively investigated during the last decade, mainly motivated by the development of string theory. A remarkable feature of the braneworld is that it modifies the Einstein equations locally and non-locally, leading to an effective energy-momentum tensor. These modifications have important consequences for cosmology [3], since significant deviations from Einstein gravity could have occurred at very high energies in the early universe. In particular, in brane cosmology, the expansion rate of the universe H scales with the energy density ρ as $H \propto \rho$, whereas this dependence is $H \propto \rho^{1/2}$ in standard cosmology. This high-energy behaviour, which is generic and not specific to RS braneworld scenarios, may affect early universe phenomena, such as inflation [4] and the generation of the cosmological baryon asymmetry [5–8].

In the RS type-II brane model, the bulk geometry is curved and the brane is endowed with a tension that is fine-tuned against the bulk cosmological constant to ensure a flat Minkowski space-time in the brane. The brane tension λ relates the Planck masses, M_P and M_5 , in four and five dimensions, respectively, via the equation $\lambda = 3M_5^6/(4\pi M_P^2)$, where $M_P = 1.22 \times 10^{19}$ GeV. Successful big bang nucleosynthesis requires that the change in the expansion rate due to the new terms in the Friedmann equation be sufficiently small at scales $\sim \mathcal{O}(\text{MeV})$. A more stringent bound can be obtained by requiring the theory to reduce to Newtonian gravity on scales larger than 1 mm [4].

Modifications to Einstein gravity are also relevant in the vicinity of massive compact objects as black holes and neutron (quark, hybrid) stars. Compact stars are therefore a special laboratory to look for possible modifications of general relativity (GR) and to test extra dimensions [9]. From the existence and stability of such astrophysical objects, one expects additional constraints on the parameters of alternative theories of gravity [10–15]. In particular, it has been shown that neutron stars put a lower bound on the brane tension λ , which is stronger than the bound coming from big bang nucleosynthesis, although weaker than the experimental Newton law limit [10]. Furthermore, the well-known compactness limit $GM/R \leq 4/9$ [16], obtained in GR by requiring the finiteness of pressure at the centre of a uniform star, is reduced by high-energy 5D gravity effects.

The macroscopic properties of compact stars also crucially depend on the constituent matter in the star interior. More precisely, star masses and radii are determined by the equation of state (EOS) of matter, i.e. by the relation $p(\rho)$ between the pressure and the energy density inside the star. In the absence of a unique framework to describe the physics of compact stars, several approaches can be adopted for the determination of the EOS. For instance, it can be reconstructed from mass-radius measurements [17–19]. Alternatively, one can resort to theoretical calculations based on chiral effective field theories and obtain stringent constraints for the neutron star radii [20], when combined with mass measurements.

In our analysis, the non-local “dark” components [3, 13] arising from the bulk Weyl tensor are modelled via the simple linear proportionality relation $\mathcal{P} = w\mathcal{U}$ between the dark energy \mathcal{U} and dark pressure \mathcal{P} . Such a functional form follows, for instance, from the requirement that the vacuum on the brane admits a one-parameter group of conformal motions and the field equations are invariant with respect to the Lie group of homologous transformations [21]. The above relation has also been used in Ref. [11] to study the junction conditions between the interior and exterior of static and spherically symmetric stars on the brane. Recently, it has been employed in the study of the mass-radius relation of some hadronic stars, hybrid stars (HS) and quark stars (QS) in the braneworld [14]. In a different context, this type of state-like relation is commonly assumed in cosmology to describe the matter content of the universe at different epochs ($w = 1/3$ for radiation domination, $w = 0$ for a matter dominated universe, and $w = -1$ for a cosmological constant).

The purpose of the present work is two-fold. First we study the limits coming from general relativity, finiteness of pressure and causality, applied to compact objects in the braneworld. In particular, assuming a Schwarzschild star interior and a pure causal EOS, we shall derive a brane-modified causality limit that depends on the brane tension, and which is more restrictive as λ decreases. The case of a vanishing dark pressure with a non-vanishing dark density will be also considered. Then we study compact stars in the RS type-II braneworld in order to establish limits on the parameters of the model. Our analysis is based on astrophysical observations and we use representative EOS to describe matter in the star interior. We shall consider a simple polytropic EOS for pure neutron matter, while for quark matter we shall employ the well-known MIT bag model [22]. We shall also consider a hybrid EOS [23] to study hybrid stars, i.e., stars with a hadronic outer region surrounding a quark (or mixed hadron-quark) inner core. The study of the macroscopic stellar properties is carried out through the solution of the Tolman-Oppenheimer-Volkoff (TOV) equations, properly modified to include local and non-local bulk effects. As it turns out, the local and non-local bulk corrections to the energy-momentum tensor play a crucial role in the stability of compact stars on the brane and in establishing agreement with observational constraints.

The paper is organised as follows. In section 2 we present and briefly discuss the TOV equations on the brane. The compactness limits in the braneworld are summarised in section 3 and a new causality limit is derived requiring the subluminality of the EOS for matter inside the compact star. In section 4, we present the brane TOV solutions for several representative EOS. The predicted mass-radius relations are then compared with the observational constraints. Finally, our concluding remarks are given in section 5.

2 TOV equations on the brane

The field equations induced on the brane have the form [3]

$$G_{\mu\nu} = R_{\mu\nu} - \frac{1}{2}Rg_{\mu\nu} = \kappa^2 T_{\mu\nu} + \frac{6\kappa^2}{\lambda} \mathcal{S}_{\mu\nu} - \mathcal{E}_{\mu\nu}, \quad (2.1)$$

where $G_{\mu\nu}$ is the usual Einstein tensor, $\kappa^2 = 8\pi G$, and $T_{\mu\nu}$ is the standard energy-momentum tensor.¹ For a spherically symmetric star, the metric in static coordinates is given by

$$ds^2 = -e^{2\Phi(r)} dt^2 + e^{2\Lambda(r)} dr^2 + r^2 (d\theta^2 + \sin^2 \theta d\phi^2). \quad (2.2)$$

The tensors $\mathcal{S}_{\mu\nu}$ and $\mathcal{E}_{\mu\nu}$ encode the local and non-local bulk corrections, respectively. For a perfect fluid, the expressions for $T_{\mu\nu}$ and $\mathcal{S}_{\mu\nu}$ are given by [3]

$$T_{\mu\nu} = \rho u_\mu u_\nu + p (g_{\mu\nu} + u_\mu u_\nu) \quad (2.3)$$

and

$$\mathcal{S}_{\mu\nu} = \frac{1}{12} \rho^2 u_\mu u_\nu + \frac{1}{12} \rho(\rho + 2p)(g_{\mu\nu} + u_\mu u_\nu), \quad (2.4)$$

where u^μ is the four-velocity of the fluid. The tensor $\mathcal{E}_{\mu\nu}$ reduces to the form

$$\mathcal{E}_{\mu\nu} = -\frac{6}{\kappa^2 \lambda} \left[\mathcal{U} u_\mu u_\nu + \mathcal{P} r_\mu r_\nu + \frac{1}{3} (\mathcal{U} - \mathcal{P}) (g_{\mu\nu} + u_\mu u_\nu) \right], \quad (2.5)$$

for the case of a static spherical symmetry. Here, r_μ is a unit radial vector, \mathcal{U} is the non-local energy density (dark radiation) and \mathcal{P} is the non-local pressure (dark pressure) on the brane. From eqs. (2.1) and (2.5), we see that standard 4D general relativity is recovered in the limit $\lambda \rightarrow \infty$.

Solving Einstein's equations for a perfect fluid matter, the following modified TOV equations are obtained on the brane:

$$\frac{dm}{dr} = 4\pi r^2 \rho_{\text{eff}}, \quad (2.6)$$

$$\frac{dp}{dr} = -(\rho + p) \frac{d\Phi}{dr}, \quad (2.7)$$

$$\frac{d\Phi}{dr} = \frac{2Gm + \kappa^2 r^3 [p_{\text{eff}} + (4\mathcal{P})/(\kappa^4 \lambda)]}{2r(r - 2Gm)}, \quad (2.8)$$

$$\frac{d\mathcal{U}}{dr} = -\frac{1}{2} \kappa^4 (\rho + p) \frac{d\rho}{dr} - 2 \frac{d\mathcal{P}}{dr} - \frac{6}{r} \mathcal{P} - (2\mathcal{P} + 4\mathcal{U}) \frac{d\Phi}{dr}, \quad (2.9)$$

where

$$\rho_{\text{eff}} = \rho_{\text{loc}} + \frac{6}{\kappa^4 \lambda} \mathcal{U}, \quad p_{\text{eff}} = p_{\text{loc}} + \frac{2}{\kappa^4 \lambda} \mathcal{U}. \quad (2.10)$$

In the above expressions,

$$\rho_{\text{loc}} = \rho + \frac{\rho^2}{2\lambda}, \quad p_{\text{loc}} = p + \frac{p\rho}{\lambda} + \frac{\rho^2}{2\lambda}, \quad (2.11)$$

denote the effective local matter density and pressure, respectively. In order to solve the system of differential equations (2.6)-(2.9), an equation of state $p(\rho)$ for matter and a relation

¹Hereafter, we use a system of natural units with $c = 1$.

$\mathcal{P}(\mathcal{U})$ are required. As explained before, we shall assume the simplest state-like relation $\mathcal{P} = w\mathcal{U}$. With this choice, eqs. (2.6)-(2.9) become

$$\frac{dm}{dr} = 4\pi r^2 \rho_{\text{eff}}, \quad (2.12)$$

$$\frac{dp}{dr} = -(\rho + p) \frac{d\Phi}{dr}, \quad (2.13)$$

$$\frac{d\Phi}{dr} = \frac{2Gm + \kappa^2 r^3 [p_{\text{eff}} + (4w\mathcal{U})/(\kappa^4\lambda)]}{2r(r - 2Gm)}, \quad (2.14)$$

$$\frac{d\mathcal{U}}{dr} = -\frac{2}{1+2w} \left[\frac{\kappa^4}{4} (\rho + p) \frac{d\rho}{dr} + \frac{3w}{r} \mathcal{U} + (w+2) \mathcal{U} \frac{d\Phi}{dr} \right], \quad (2.15)$$

where the last equation holds for $w \neq -1/2$. The case $w = -1/2$ should be treated separately. Solving for \mathcal{U} in eq. (2.9) and using (2.8), we obtain

$$\mathcal{U}(r) = \frac{\kappa^4 (\rho + p)^2}{6v_s^2} \frac{2Gm + \kappa^2 r^3 p_{\text{loc}}}{2(3Gm - r) + \kappa^2 r^3 p_{\text{loc}}}, \quad (w = -1/2), \quad (2.16)$$

where v_s is the speed of sound,

$$v_s^2 = \frac{dp}{d\rho}. \quad (2.17)$$

To integrate the TOV equations, we need appropriate initial conditions at the centre of the star. As in general relativity, we assume that the enclosed mass is zero at the centre, $m(0) = 0$, and that $p(0) = p_c$, where p_c is the central pressure. At the stellar surface, we require $p(R) = 0$, i.e. a vanishing pressure, which corresponds to a star mass $m(R) = M$. As for the dark component \mathcal{U} , we shall assume that $\mathcal{U}(0) = 0$. We remark that different initial conditions for the dark energy density \mathcal{U} can be chosen. They could be given either at the centre of the star or at its surface. In the latter case, a shooting method is required for the integration of the system of equations [15]. The boundary condition chosen here, i.e. a vanishing dark density at the centre, is the simplest choice. Note also that if $w = -1/2$, the value of \mathcal{U} at the centre is obtained directly from eq. (2.16).

The system (2.12)-(2.15) must be supplemented with the Israel-Darmois junction conditions [24, 25] at the stellar surface. On the brane, this leads to the matching condition

$$\left[p_{\text{eff}} + \frac{4}{\kappa^4 \lambda} \mathcal{P} \right]_{\text{surf}} = 0, \quad (2.18)$$

where $[f]_{\text{surf}} \equiv f(R^+) - f(R^-)$, and the superscripts $+$ and $-$ refer to quantities defined outside and inside the star, respectively. The requirement $p(R) = 0$ at the surface then implies

$$\frac{\kappa^4}{4} \rho^2(R) + \mathcal{U}^-(R) + 2\mathcal{P}^-(R) = \mathcal{U}^+(R) + 2\mathcal{P}^+(R). \quad (2.19)$$

In the absence of any Weyl stress in the interior, we have $\mathcal{P}^- = \mathcal{U}^- = 0$ and eq. (2.19) implies that the exterior must be non-Schwarzschild, provided that the energy density ρ does not vanish at the surface. The same conclusion holds if $w = -1/2$, since in this case $\mathcal{U}^-(R) + 2\mathcal{P}^-(R) = 0$. On the other hand, if $\rho(R) \neq 0$ and the exterior is Schwarzschild ($\mathcal{P}^+ = \mathcal{U}^+ = 0$), then the interior is necessarily non-Schwarzschild. We also note that, in the braneworld, the TOV equations admit asymptotically flat exterior solutions different from the Schwarzschild solution. In what follows, our analysis is restricted to solutions in the star interior with generic dark energy and dark pressure components obeying the EOS relation $\mathcal{P} = w\mathcal{U}$. The discussion of possible exterior solutions is beyond the scope of this work.

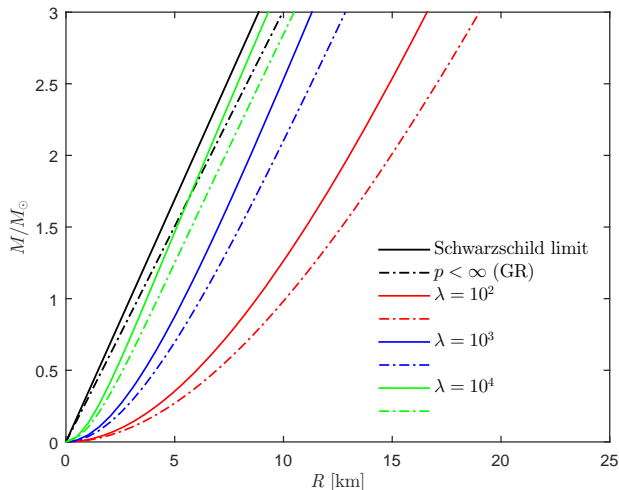


Figure 1. General relativity and pressure finiteness limits on the brane, assuming a Schwarzschild interior with $\mathcal{P} = \mathcal{U} = 0$. The brane tension λ is given in units of MeV/fm^3 .

3 Compactness limits in the braneworld

In this section, we revisit the compactness limits on a uniform star coming from general relativity and the requirement of the finiteness of pressure. We shall also derive a brane-modified causality limit for the existence of stable stars.

Assuming a uniform density and a Schwarzschild interior ($\mathcal{P} = \mathcal{U} = 0$), the high-energy brane corrections are local. In this case, an astrophysical lower limit on λ , independent of the Newton-law and cosmological limits, can be established for all uniform stars [10]:

$$\lambda \geq \frac{GM\rho}{R - 2GM}, \quad (3.1)$$

with $\rho = 3M/(4\pi R^3)$. For a positive brane tension, this implies $R > 2GM$, so that the Schwarzschild radius remains a limiting radius. Below the astrophysical limit (3.1), stable neutron stars cannot exist on the brane. This bound is much stronger than the cosmological nucleosynthesis constraint, but turns out to be weaker than the Newton-law lower bound. From eq. (3.1), we find the following upper bound for the mass:

$$M(R) = \frac{2R^2}{3} \left(\sqrt{\pi\lambda(3G^{-1} + 4\pi\lambda R^2)} - 2\pi\lambda R \right). \quad (3.2)$$

As expected, in the limit $\lambda \rightarrow \infty$, we recover the Schwarzschild limit of GR:

$$M(R) = \frac{1}{2} \frac{R}{G}. \quad (3.3)$$

The astrophysical bound given by eq. (3.2) is illustrated in figure 1 for different values of λ (solid lines). As can be seen from the figure, brane corrections to the compactness limit would be significant for $\lambda \lesssim 10^4 \text{ MeV}/\text{fm}^3$, leading to a less compact star in the braneworld, when compared to the general relativity case.

Another important limit comes from requiring the pressure inside the compact object to be finite. Since the pressure decreases with the radius r , this condition is equivalent to

the requirement of a positive and finite pressure at the centre of the star. This gives the constraint [10]

$$\frac{GM}{R} \leq \frac{4}{9} \frac{1 + 7\rho/4\lambda + 5\rho^2/8\lambda^2}{(1 + \rho/\lambda)^2(1 + \rho/2\lambda)}. \quad (3.4)$$

Solving for M to find the maximum mass, we obtain

$$M(R) = \frac{4\sqrt{\pi}R^2}{9G} \left[-2\sqrt{\pi}G\lambda R + \sqrt{G\lambda(5 + 4\pi G\lambda R^2)} \cos\left(\frac{1}{3}\tan^{-1}x\right) \right], \quad (3.5)$$

where

$$x = \frac{(125G^{-1}\lambda^{-1} + 264\pi R^2 + 144\pi^2 G\lambda R^4)^{1/2}}{2\sqrt{\pi}R(3 + 4\pi G\lambda R^2)}. \quad (3.6)$$

In the limit $\lambda \rightarrow \infty$, we recover the pressure finiteness limit of GR

$$M(R) = \frac{4}{9} \frac{R}{G}. \quad (3.7)$$

The curve defined by eq. (3.5) is presented in figure 1 for different values of the brane tension (dot-dashed lines). As in the case of the Schwarzschild limit, high-energy braneworld corrections are significant for $\lambda \lesssim 10^4$ MeV/fm³. We also note that for a given radius R the maximum mass allowed by the bound (3.5) is lower than that coming from the limit in eq. (3.2).

A third relevant constraint on the maximum star mass comes from causality, i.e. from requiring the subluminality of the EOS, i.e. $v_s^2 \leq 1$. The bound obtained from this condition is controlled by the stiffness of the matter EOS, and several limits have been derived in the literature [26–28] (see also [17] for a review). In particular, a stringent causal limit has been obtained in Ref. [28], based on the “minimum period” EOS

$$p = \begin{cases} 0, & \rho < \rho_s, \\ \rho - \rho_s, & \rho \geq \rho_s, \end{cases} \quad (3.8)$$

where ρ_s is the surface energy density. This EOS corresponds to maximal stiffness at high densities and minimal stiffness at low densities, thus supporting the largest mass with the smallest radius. In general relativity, such EOS also implies that the maximum value of the mass scales with the radius as $M \propto R$. The numerical integration of the TOV equations for various initial values of the central pressure p_c then leads to the GR relation [28]

$$R \simeq 2.82 GM. \quad (3.9)$$

As we shall show next, this compactness limit is modified in the braneworld.

From eqs. (2.10) and (2.11), and using the conservation equations for ρ and \mathcal{U} , the effective speed of sound is obtained as

$$v_{s,\text{eff}}^2 \equiv \frac{dp_{\text{eff}}}{d\rho_{\text{eff}}} = \frac{v_s^2(1 + \rho/\lambda) + (\rho + p)/\lambda + v_{\mathcal{U}}^2}{1 + \rho/\lambda + 3v_{\mathcal{U}}^2}, \quad (3.10)$$

where

$$v_{\mathcal{U}}^2 = \frac{8}{3\kappa^4\lambda} \frac{\mathcal{U}}{\rho + p}. \quad (3.11)$$

As expected, in the limit $\lambda \rightarrow \infty$, we have $v_{s,\text{eff}} = v_s$. Note also that $v_{\mathcal{U}}^2$ is not necessarily a positive number, since the Weyl energy density can be negative. Moreover, when the radiation term $v_{\mathcal{U}}$ dominates over the matter components, one has $v_{s,\text{eff}}^2 \simeq 1/3$.

Let us consider a star with a Schwarzschild interior ($\mathcal{P} = \mathcal{U} = 0$). In this case, $v_{\mathcal{U}} = 0$ and from eq. (3.10) we obtain the effective speed of sound

$$v_{s,\text{eff}}^2 = v_s^2 + \frac{\rho + p}{\rho + \lambda}. \quad (3.12)$$

Thus, in the braneworld, the minimum period EOS in eq. (3.8) always lead to an effective speed of sound $v_{s,\text{eff}} > 1$, since for such EOS one has $v_s = 1$. We then conclude that in order to comply with the causality limit $v_{s,\text{eff}} \leq 1$ inside a star with a Schwarzschild interior, any linear EOS relation of the form $p = a(\rho - \rho_s)$ requires $0 < a < 1$. This in turn leads to a lower bound on the brane tension,

$$\lambda > \frac{a(2\rho - \rho_s)}{1 - a}. \quad (3.13)$$

Let us take, for instance, a neutron star with $\rho \sim \rho_0 \gg \rho_s$, where $\rho_0 = 2.7 \times 10^{14} \text{ g/cm}^3 \simeq 150 \text{ MeV/fm}^3$ is the nuclear saturation density. Using a radiation-like EOS with $a = 1/3$, we estimate $\lambda \gtrsim \rho_0$. At the star surface, the less restrictive bound $\lambda > \rho_s/2$ must hold.

Consider now the case of a Schwarzschild exterior and a star interior with $\mathcal{P} = 0$ (i.e. $w = 0$) and $\mathcal{U} \neq 0$. In this case, the boundary condition (2.19) yields a negative dark radiation density at the star surface. We obtain $\mathcal{U} = -\kappa^4 \rho_s^2/4$, so that $v_{\mathcal{U}}^2 = -2\rho_s/(3\lambda)$ at the surface. From eq. (3.10) we then find

$$v_{s,\text{eff}}^2 = \frac{v_s^2(1 + \rho_s/\lambda) + \rho_s/(3\lambda)}{1 - \rho_s/\lambda}. \quad (3.14)$$

Requiring $v_{s,\text{eff}} \leq 1$, the constraint

$$\lambda > \frac{(4/3 + a)\rho_s}{1 - a}, \quad (3.15)$$

with $a < 1$, is obtained. For $a = 1/3$, this gives the lower bound $\lambda > 5\rho_s/2$.

Bearing in mind the limitations of the causal EOS given in eq. (3.8), we shall nevertheless use this relation to illustrate how the corrections due to brane effects modify the GR compactness limit of eq. (3.9). Solving numerically the system of equations (2.12)-(2.15), from the star centre until the surface, we can determine the maximum star mass. The results are presented in figure 2 (left plot) for different values of the brane tension λ . Significant deviations from the causality limit in GR (black solid line) occur for $\lambda \lesssim 10^4 \text{ MeV/fm}^3$, as can be seen from the curves for maximal masses depicted in the figure.

In order to illustrate the sensitivity of the causality limit to non-local bulk effects, we consider next the case with $w = 0$. Following the same numerical procedure, we obtain the maximal masses (minimal radii) presented in the second column of table 1. Remarkably, in this case, the maximum mass can be approximated by a straight line, $M \simeq \alpha R/G$, with a slope α that increases as the brane tension λ increases, reaching the GR limit (3.9) when $\lambda \rightarrow \infty$.

It has been recently conjectured that the speed of sound should satisfy the bound $v_s \leq 1/\sqrt{3}$ in any medium [29]. It is well known that this bound is saturated in conformal

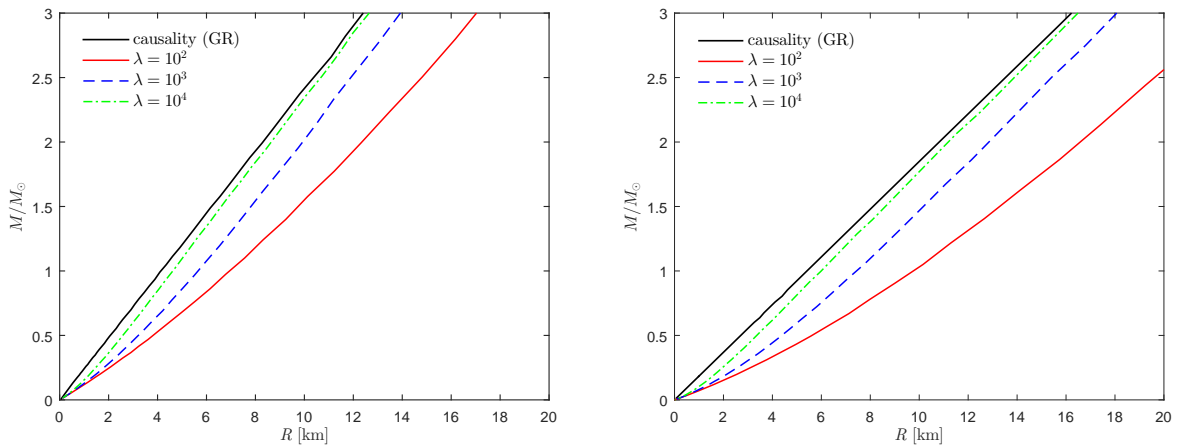


Figure 2. Causality constraint on the brane, obtained from the causal EOS of eq. (3.8) (left plot) and eq. (3.16) (right plot). A Schwarzschild interior with $\mathcal{P} = \mathcal{U} = 0$ is assumed. The brane tension λ is given in units of MeV/fm^3 .

λ [MeV/fm^3]	$v_s \leq 1$	$v_s \leq 1/\sqrt{3}$
	$R/(GM)$	$R/(GM)$
10	3.73	4.95
10^2	3.46	4.61
10^3	3.04	4.10
10^4	2.85	3.73
∞ (GR)	2.82	3.66

Table 1. Causality limit in the braneworld for two causal EOS (with $v_s \leq 1$ and $v_s \leq 1/\sqrt{3}$), assuming a vanishing dark radiation pressure ($\mathcal{P} = 0$) and a non-zero dark energy density \mathcal{U} in the star interior. The minimum radius is approximately described by a straight line with a slope that varies with the brane tension.

theories, including non-interacting massless gases for which $p = \rho/3$. The limit also applies to non-relativistic and weakly coupled theories, and is respected by several strongly coupled theories. If such a bound actually holds for the speed of sound, it would modify the causality limit for compact astrophysical objects. In particular, it has been pointed out that the existence of neutron stars with $M \sim 2M_\odot$, combined with the knowledge of the EOS of hadronic matter at low densities, is in strong tension with this bound [29].

To illustrate the implications of the bound $v_s \leq 1/\sqrt{3}$ for the stability of compact stars, let us consider the minimal causal EOS

$$p = \begin{cases} 0, & \rho < \rho_s \\ (\rho - \rho_s)/3, & \rho \geq \rho_s, \end{cases} \quad (3.16)$$

which saturates the bound.² We should keep in mind that the above causal EOS violates the

²Note that the simple EOS of the well-known MIT bag model (with massless quarks and no strong coupling constant) has also this form. In this case, the parameter ρ_s is associated to the bag constant, $\rho_s \equiv 4B$.

causality limit $v_{s,\text{eff}} \leq 1/\sqrt{3}$ for a Schwarzschild interior. The numerical integration of the TOV equations of GR implies the causality relation

$$R \simeq 3.66 GM, \quad (3.17)$$

which is more restrictive than the bound (3.9). The inclusion of brane corrections leads to modifications to this limit. For the case of a Schwarzschild interior, the results are shown in figure 2 (right plot). Once again, significant deviations from the causality limit of GR take place for $\lambda \lesssim 10^4 \text{ MeV/fm}^3$. We have also considered the case with $\mathcal{P} = 0$ and $\mathcal{U} \neq 0$. The results are given in the last column of table 1. As before, the minimum radius is well approximated by a straight line whose slope varies with the brane tension. We note that, for any given value of λ , the constraint obtained from requiring $v_s \leq 1/\sqrt{3}$ is always stronger than the one previously found under the assumption $v_s \leq 1$.

4 Brane TOV solutions and observational constraints

Due to the uncertainties in the description of the many-body interactions and the nuclear symmetry energy, as well as our lack of knowledge of the precise nature of strong interactions, the EOS of dense matter above the nuclear saturation density ρ_0 is largely unknown. Depending on the matter composition in the neutron star interior, three main types of equations of state have been commonly used, namely, EOS for normal dense matter, pure quark matter or hybrid matter.

In the case of normal dense matter, neutron stars are supported against gravitational collapse by neutron degeneracy. The EOS takes into account nucleon-nucleon interactions and is characterised by a vanishing pressure at null densities. For hybrid stars, the EOS is usually softened at high densities by adding hadronic or pure quark matter at the inner core of the star, which leads to a phase transition at a given critical density. Normal and hybrid EOS do not lead to stringent bounds for the star radii, which in principle can be large ($\sim 100 \text{ km}$). On the other hand, pure quark stars are conjectured to be mainly composed of strange quark matter (SQM) in the ground state, with a vanishing pressure at non-zero densities. For such stars the maximum radius is not so large ($\sim 10 \text{ km}$). In all three EOS cases, the mass-radius relation predicts a maximum mass M_{max} . While typically $M_{max} \lesssim 2M_\odot$ for hybrid and strange quark EOS, maximum masses up to $2.5M_\odot$ can be reached with normal matter EOS.

From the astrophysical viewpoint, an important aspect in the study of stellar configurations is their stability. A necessary condition for the stability of a compact star is given by the so-called static criterion

$$\frac{dM}{d\rho_c} > 0. \quad (4.1)$$

In other words, a compact star is stable if its mass M increases with growing central density $\rho_c = \rho(p_c)$. Although the stability analysis is usually quite involved, some simple criteria can be formulated based on the mass-radius configurations and their stability with respect to radial oscillations (see e.g. [30] and references therein). At each extremum (critical point) of the $M(R)$ curve, it is assumed that only one radial mode changes its stability from stable to unstable or, vice versa, from unstable to stable. Furthermore, at any critical point, a mode becomes unstable (stable) if and only if the curve bends counterclockwise (clockwise). Finally, a mode with an even (odd) number of radial nodes is said to change its stability if and only if $dR/d\rho_c > 0$ ($dR/d\rho_c < 0$) at the critical point. Using the above criteria, the stability of a given stellar configuration can be easily checked.

In order to confront different EOS with current mass and radius measurements, we shall use the following observational constraints. For neutron star radii, we consider the range

$$7.6 \text{ km} \leq R \leq 13.9 \text{ km}, \quad (4.2)$$

where the lower bound follows from the measurement of the neutron star radius using the thermal spectra from quiescent low-mass X-ray binaries inside globular clusters [31] and the upper limit is taken from the analysis of Ref. [20], based on the chiral effective theory. For the allowed range of the star masses, we adopt the bounds

$$1.39M_{\odot} \leq M \leq 2.05M_{\odot}, \quad (4.3)$$

where the minimum value corresponds to the Chandrasekhar limit and the maximum value is obtained from recent radio-timing observations of the pulsar PSR J0348+0432 [32].

In the braneworld, the macroscopic properties of stable stellar configurations are controlled not only by the matter EOS but also by high-energy brane effects, characterised in our setup by the brane tension and the assumed dark EOS. Next we analyse the implications of these effects on the mass-radius relations of stable compact stars for the three classes of EOS mentioned above. In our analysis, we shall take into account the stability criteria as well as the causality limit $v_{s,\text{eff}} \leq 1$, based on the effective speed of sound defined in eq. (3.10).

4.1 Pure neutron stars with nucleon-nucleon interactions

Let us study first the example of a pure neutron star (PNS) with nucleon-nucleon interactions. These interactions can be modelled in the EOS of matter by a simple nuclear potential describing the relevant features of nuclear matter. In this case, the EOS can be described by a simple polytropic form. We consider

$$\rho(p) = A_0 \epsilon_0^{1/2} p^{1/2}, \quad (4.4)$$

where $A_0 = 0.8642$ and $\epsilon_0 = m_n^4 / (3\pi^2) = 3.4162 \times 10^3 \text{ MeV/fm}^3$ [33]; ρ and p are given in units of MeV/fm^3 . The above EOS is supplemented at low densities with the well-known Baym-Pethick-Sutherland (BPS) model [34].

We can then proceed to solve the system of brane TOV equations for different initial values of the central pressure p_c in order to determine the mass-radius relation for such neutron stars. We consider first the case of a dark EOS with $w = 0$. The results are presented in figures 3 and 4, where the stable mass-radius configurations, i.e. those that verify the stability criteria and obey the causality limit $v_{s,\text{eff}} \leq 1$, are given. In all plots, the small circles denote the maximum mass M_{max} (in units of solar masses M_{\odot}) for the corresponding star configuration. The shaded grey areas correspond to the observational constraints of eqs. (4.2) and (4.3), where the dark grey band is the mass range of the pulsar PSR J0348+0432 [32].

As can be seen from the left panel of figure 3, the maximum mass and the corresponding star radius decrease as λ decreases, so that requiring agreement with observational constraints leads to a lower bound on the brane tension, $\lambda \gtrsim 10^3 \text{ MeV/fm}^3$. The star radii lie in the range 8–12 km. Furthermore, from the right panel of the figure, we conclude that the central energy density ρ_c required to achieve such maximum mass configurations is always less than that of GR, namely, $\rho_c \lesssim 7\rho_0$.

In figure 5, the maximum star mass is given as a function of the brane tension (left panel) and the dark EOS parameter w (right panel). From the figure we conclude that the

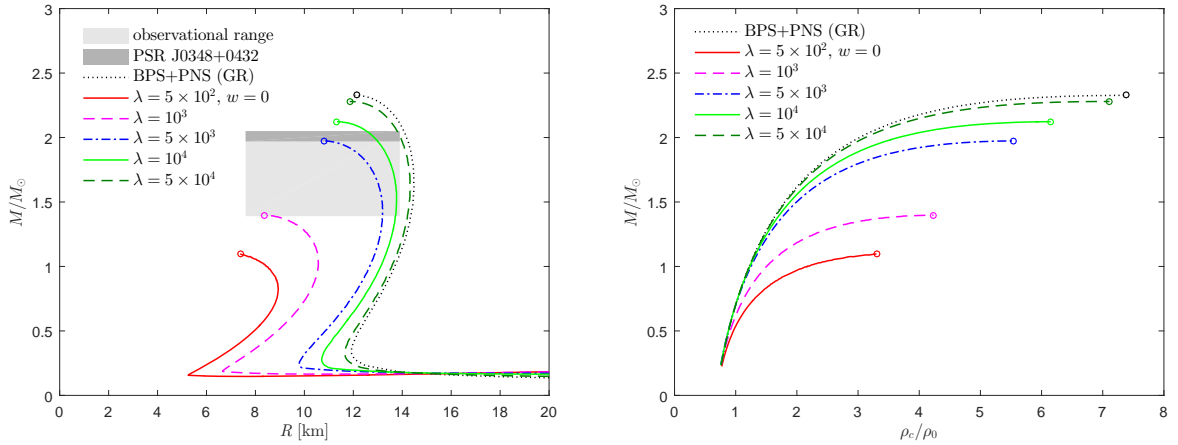


Figure 3. Left plot: Mass-radius relation for the BPS+PNS EOS. The curves are given for different values of the brane tension λ (in MeV/fm^3), assuming a vanishing dark pressure in the star interior ($w = 0$). Right plot: The mass of the star versus the central energy density ρ_c (in units of the nuclear saturation density ρ_0).

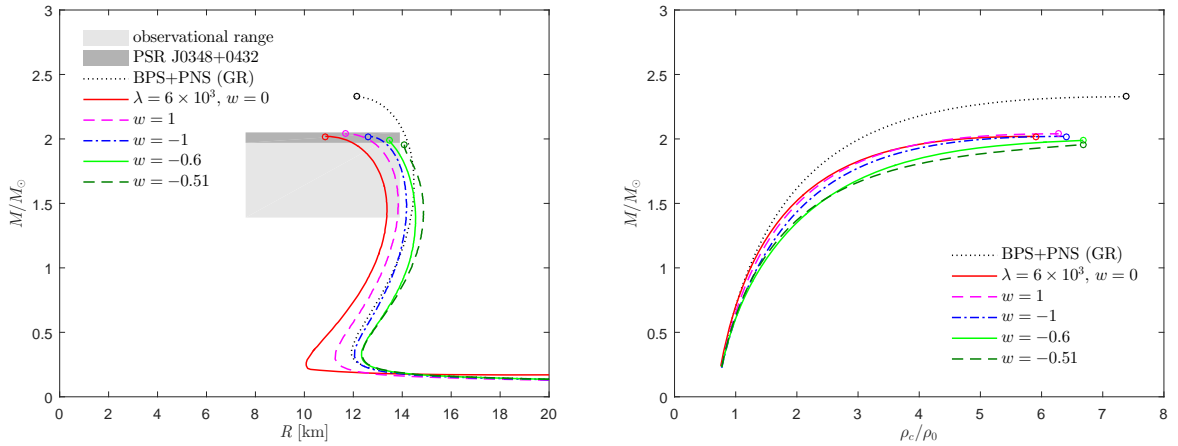


Figure 4. Left plot: Mass-radius relation for the BPS+PNS EOS. The curves are given for different values of the dark EOS parameter w and $\lambda = 6 \times 10^3 \text{ MeV}/\text{fm}^3$. Right plot: The mass of the star versus the central energy density ρ_c (in units of ρ_0).

maximum star mass predicted for this type of EOS is compatible with observations provided that $\lambda \gtrsim 6 \times 10^2 \text{ MeV}/\text{fm}^3$. We also note that, for a given value of λ , the largest mass is always attained for the TOV solution that corresponds to a Schwarzschild interior. For $w \gtrsim -0.1$, the value of M_{max} remains practically constant with the variation of w , depending only on the value of λ . A similar behaviour is observed for $w \lesssim -0.5$. However, for $-0.3 < w < -0.1$, the maximum mass is quite sensitive to w , as it becomes evident in the right panel of figure 5.

4.2 Quark stars

It has been conjectured that strange quark matter could be the true ground state of strongly interacting matter at zero pressure and temperature [35]. If this possibility actually exists,

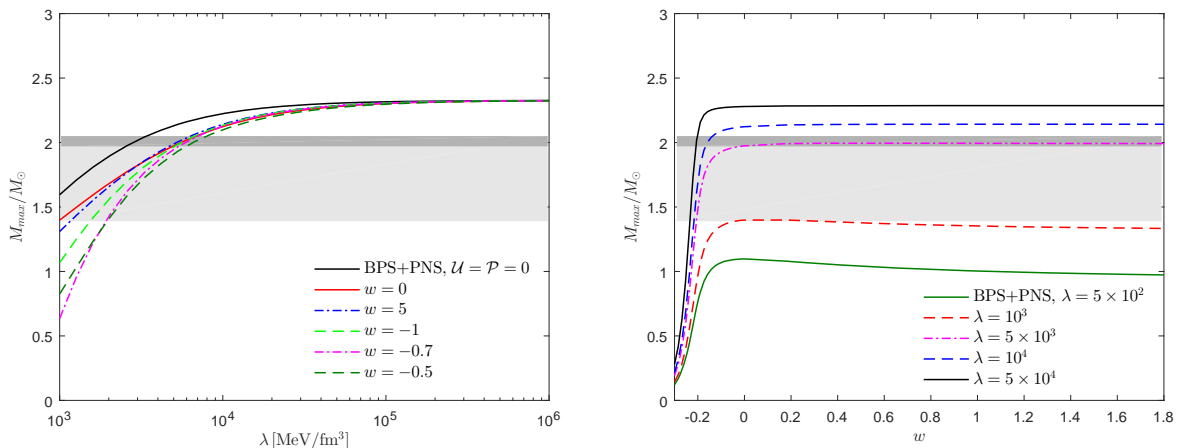


Figure 5. Left plot: Maximum neutron star mass as a function of the brane tension for different values of the dark EOS parameter w . Right plot: Maximum star mass as a function of the dark EOS parameter w for different values of the brane tension.

it would open the window for the existence of compact stellar objects totally composed of SQM [36]. To describe the EOS inside such stars, we consider the well-known MIT bag model based on the simple relation [22]

$$\rho(p) = 3p + 4B, \quad (4.5)$$

where B is the bag constant. Assuming massless quarks and neglecting the strong coupling constant, the hypothesis that three flavour quark matter has an energy per baryon lower than that of ordinary nuclei holds for $59 \text{ MeV/fm}^3 \lesssim B \lesssim 92 \text{ MeV/fm}^3$. Hereafter we take $B = 60 \text{ MeV/fm}^3$.

We follow the same procedure as before, i.e. we integrate the brane-modified TOV equations for different initial values of the central pressure p_c and determine the mass-radius relation for the corresponding quark star configuration. Our results are presented in figures 6 and 7. As shown in the left panel of figure 6, the maximum mass and the corresponding star radius decrease as λ decreases and agreement with observational constraints imposes the lower bound $\lambda \gtrsim 3 \times 10^3 \text{ MeV/fm}^3$, for $w = 0$. The allowed star radii are in the range 8–11 km. Moreover, from the right panel of the figure, we conclude that the central energy density for the maximum mass configurations is bounded by $\rho_c \lesssim 7\rho_0$.

In figure 7, we present the mass-radius relation for the case of $\lambda = 6 \times 10^3 \text{ MeV/fm}^3$ and different values of w . We notice that for certain negative values of w the mass-radius curves bend clockwise, reaching the maximum mass at relatively high central densities, $\rho_c \sim 40\rho_0$. Although such density values are higher than the maximum central density of typical bare strange stars, they are below the critical density required for the formation of a stable charm-quark star. We recall that a c -quark can be created via the weak reaction $u + d \rightarrow c + d$. Since the charm quark mass is $m_c \simeq 1.275 \text{ GeV}$ [37], the production of a quark c requires $\rho \geq \rho_{\text{crit},c} = 9m_c^4/(4\pi^2) \simeq 1.4 \times 10^{17} \text{ g/cm}^3 \simeq 5.2 \times 10^2 \rho_0$. Based on the stability analysis, it has been found in the context of GR that charm-quark stars are unstable against radial oscillations [38]. In the mass-radius plane, such an instability is manifested in the inwardly spiralling behaviour of the curves, and it is also confirmed through the calculation of the star oscillation frequencies [38].

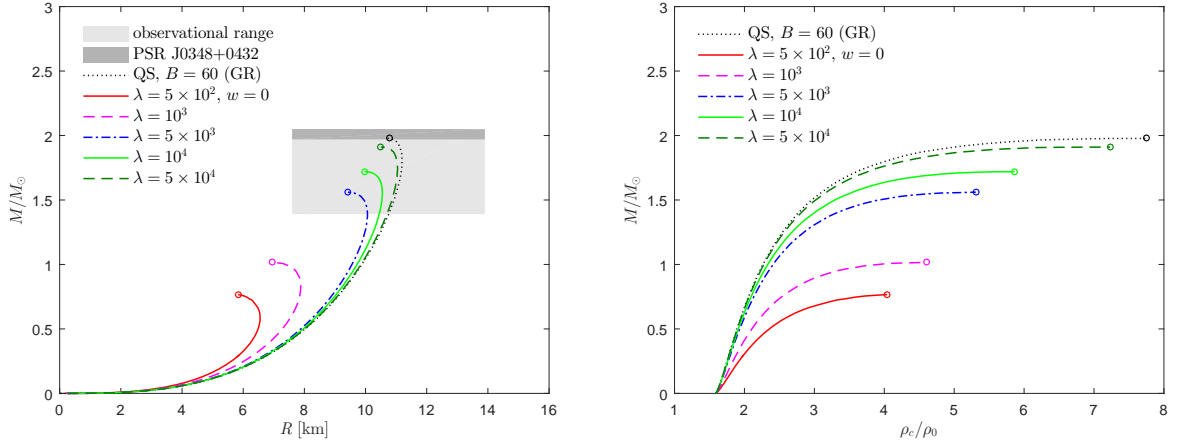


Figure 6. Left plot: Mass-radius relation for a quark star, using the MIT bag model EOS with $B = 60 \text{ MeV/fm}^3$. The curves are given for different values of the brane tension λ (in MeV/fm^3), assuming a vanishing dark pressure in the star interior ($w = 0$). Right plot: The mass of the quark star versus the central energy density ρ_c (in units of ρ_0).

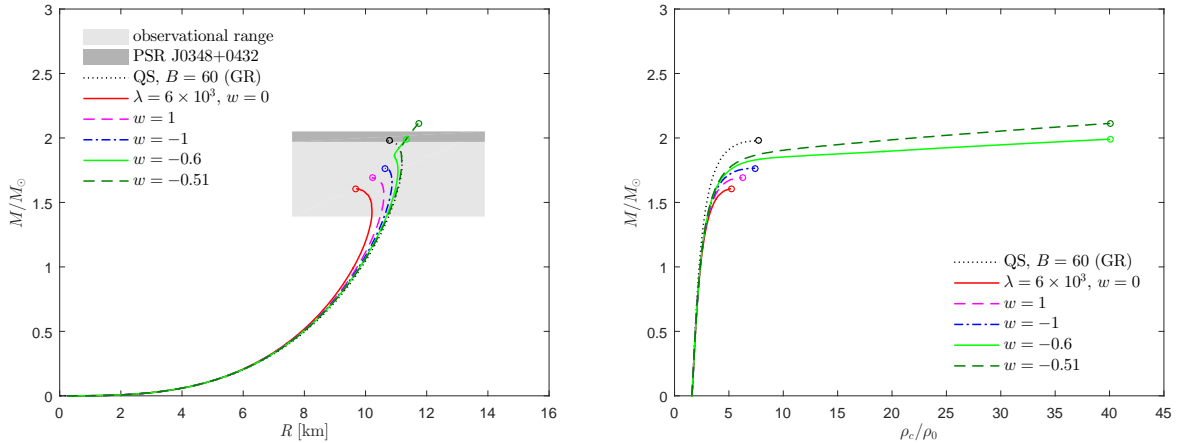


Figure 7. Left plot: Mass-radius relation for a quark star, using the MIT bag model EOS with $B = 60 \text{ MeV/fm}^3$. The curves are given for different values of the dark EOS parameter w and $\lambda = 6 \times 10^3 \text{ MeV/fm}^3$. Right plot: The mass of the quark star versus the central energy density ρ_c (in units of ρ_0).

Finally, in figure 8, the maximum star mass is presented as a function of the brane tension (left panel) and the dark EOS parameter w (right panel). We see that the maximum star mass predicted for the quark bag model is compatible with observations provided that $\lambda \gtrsim 10^3 \text{ MeV/fm}^3$. As in the case of pure neutron stars, for $w \gtrsim -0.2$, the value of M_{max} remains essentially constant with the variation of w , and depends only on the value of λ . The same conclusion holds for $w \lesssim -0.5$. In the range $-0.4 < w < -0.2$, however, the maximum mass is quite sensitive to the value of w , as seen in the right panel of figure 8.

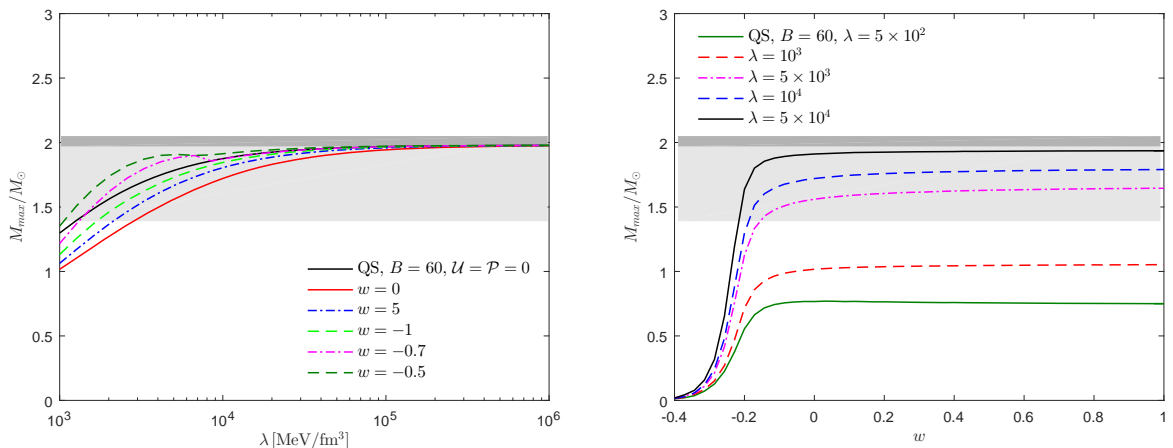


Figure 8. Left plot: Maximum quark star mass as a function of the brane tension for different values of the dark EOS parameter w . Right plot: Maximum star mass as a function of the dark EOS parameter w for different values of the brane tension.

4.3 Hybrid stars

The maximum values of the central energy densities ρ_c , obtained from EOS of purely hadronic matter, are typically in the range $5\rho_0$ – $10\rho_0$. At such densities, one expects quark degrees of freedom to play a relevant role inside compact stars. It is then natural to consider the possibility of the formation of hybrid compact objects, i.e. stars that contain a core of quark matter with a crustal of nuclear matter.

We describe a hybrid star using the following combined EOS. For the low density region, valid up to $2\rho_0$, we use the standard BPS EOS [34]. The regime of densities in the range $2\rho_0 \leq \rho \leq 4\rho_0$ will be modelled by eq. (4.4). Finally, for the core of the hybrid star, corresponding to densities $\rho > 4\rho_0$, we use the simple phenomenological parametrisation given in Ref. [23]. It consists of a power series expansion in the quark chemical potential μ ,

$$\rho = \frac{9}{4\pi^2} a_4 \mu^4 - \frac{3}{4\pi^2} a_2 \mu^2 + B, \quad (4.6)$$

$$p = \frac{3}{4\pi^2} a_4 \mu^4 - \frac{3}{4\pi^2} a_2 \mu^2 - B. \quad (4.7)$$

Besides the bag parameter B , this parametrisation contains two additional parameters, a_4 and a_2 , which are independent of μ and are related to the QCD and strange quark mass (and color superconductivity) corrections, respectively. For quark matter consisting of three flavours of free massless quarks, $a_4 = 1$ and $a_2 = 0$, so that in this case eqs. (4.6) coincide with the MIT bag model EOS (4.5). In our numerical calculations we shall take $a_4 = 0.7$, $a_2 = (180 \text{ MeV})^2$ and $B = 60 \text{ MeV/fm}^3$, which have been shown to be reasonable values [23].

For hybrid stars, we determine the mass-radius relation by the integration of the brane-modified TOV equations for different initial values of the central pressure p_c . Our results are presented in figures 9 and 10. From the left plot of figure 9, we conclude that the maximum mass and the corresponding star radius decrease as λ decreases. Furthermore, it is seen that for $\lambda \gtrsim 10^3 \text{ MeV/fm}^3$, and taking $w = 0$, the masses and radii obtained are in agreement with the observational constraints. The maximum mass is obtained for GR, $M \sim 2.1M_{\odot}$, to be compared with the value $M \sim 2.3M_{\odot}$ achieved with the pure neutron star EOS. The

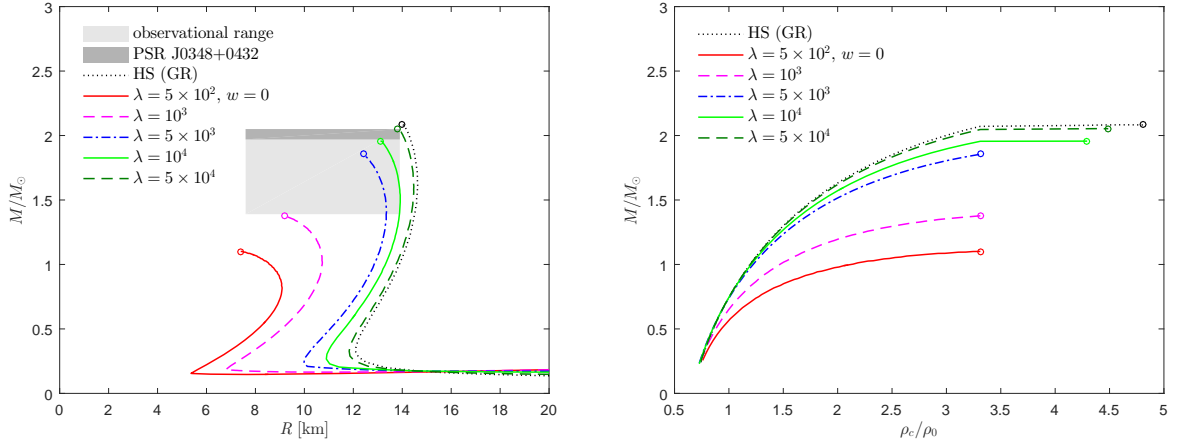


Figure 9. Left plot: Mass-radius relation for the hybrid EOS. The curves are given for different values of the brane tension λ (in MeV/fm^3), assuming a vanishing dark pressure in the star interior ($w = 0$). Right plot: The mass of the star versus the central energy density ρ_c (in units of the nuclear saturation density ρ_0).

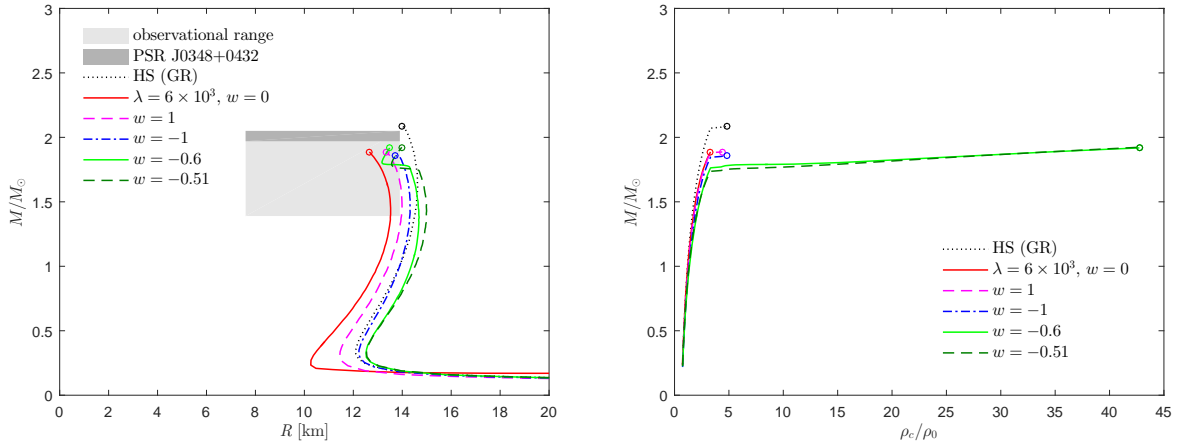


Figure 10. Left plot: Mass-radius relation for the hybrid EOS. The curves are given for different values of the dark EOS parameter w and $\lambda = 6 \times 10^3 \text{ MeV}/\text{fm}^3$. Right plot: The mass of the star versus the central energy density ρ_c (in units of ρ_0).

central energy densities are $\rho_c \lesssim 4.5\rho_0$ (right panel of figure 9). The allowed star radii are in the range 9–14 km, slightly shifted to higher values when compared to those obtained for pure neutron stars (cf. figure 3).

In figure 10, we present the mass-radius relation for the case of $\lambda = 6 \times 10^3 \text{ MeV}/\text{fm}^3$ and different values of the dark EOS parameter w . As in the case of quark stars, we notice that the clockwise bending of the mass-radius curves persists for certain negative values of w , reaching the maximum mass at relatively high central densities, $\rho_c \sim 45\rho_0$, as depicted in the right plot of figure 10.

In figure 11, the maximum star mass is plotted as a function of λ (left panel) and w (right panel). We see that the maximum star mass predicted for the hybrid star model

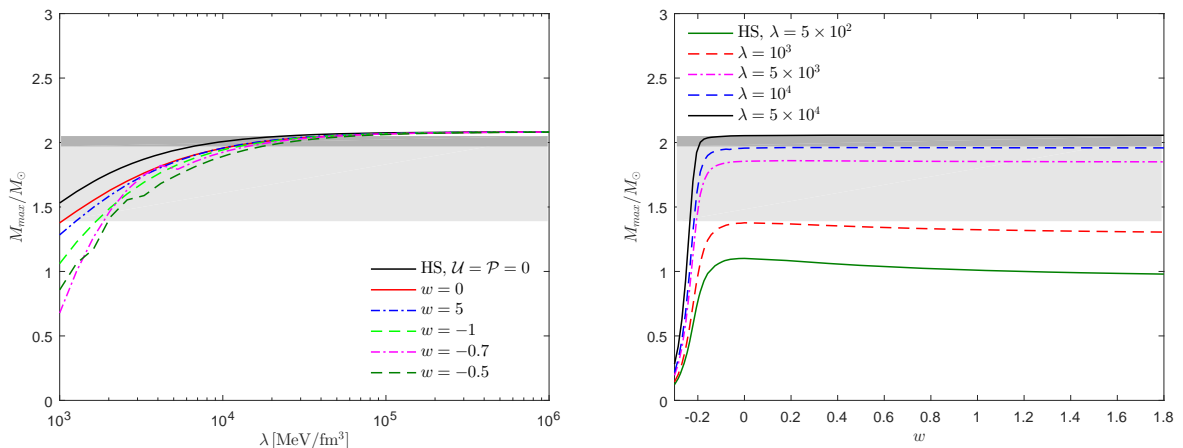


Figure 11. Left plot: Maximum hybrid star mass as a function of the brane tension for different values of the dark EOS parameter w . Right plot: Maximum star mass as a function of the dark EOS parameter w for different values of the brane tension.

is compatible with observations provided that $\lambda \gtrsim 10^3$ MeV/fm³. The behaviour of the maximum mass with w is similar to the one obtained for pure neutron and quark stars. For $w \lesssim -0.5$ and $w \gtrsim -0.2$, the value of M_{max} remains essentially constant with the variation of w , depending only on the value of λ . Yet, the maximum mass is very sensible to the variation of w in the range $-0.3 < w < -0.1$ (as in the case of pure neutron stars). This is clearly seen in the right plot of figure 11.

5 Conclusions

In this paper we have studied compact stars in the RS type-II braneworld. We have analysed the braneworld corrections to the different constraints for star masses and radii, considering compactness, causality and finite pressure at the core. We have solved the brane-modified TOV equations for different EOS that describe pure neutron stars, quarks stars and hybrid stars. We have then confront our results with recent astrophysical observations.

To study the compactness limits and the effects of the brane corrections, we have solved the TOV equations assuming a Schwarzschild star interior ($\mathcal{P} = \mathcal{U} = 0$) and a uniform star density. We have shown that the brane corrections are significant for $\lambda \lesssim 10^4$ MeV/fm³ and lead to a less compact star, when compared to the general relativity case. A λ -dependent limit was derived from the requirement of finiteness of pressure in the star core. The well-known compactness limits of general relativity are recovered in the limit $\lambda \rightarrow \infty$.

Significant deviations from the causality limit of general relativity are obtained when $\lambda \lesssim 10^4$ MeV/fm³. Similar results are found in the case of $\mathcal{P} = 0$ and $\mathcal{U} \neq 0$, i.e. for a dark EOS with $w = 0$. In the latter case, the minimum radius is well approximated by a straight line whose slope varies with the brane tension. The constraints were obtained considering two different conditions for the speed of sound in dense matter, namely, $v_s \leq 1$ and $v_s \leq 1/\sqrt{3}$. We have also derived an effective speed of sound, $v_{s,\text{eff}} = dp_{\text{eff}}/d\rho_{\text{eff}}$, which includes corrections due to local and non-local braneworld effects. The causality condition $v_{s,\text{eff}} \leq 1$ was then imposed on the different EOS in order to find stable stellar configurations.

The mass-radius relations were computed by solving the TOV equations for three different matter EOS, imposing the stability and causality criteria. The study was first done for $w = 0$ and different values of the brane tension. In all the three EOS cases, the maximum mass and the corresponding star radius decrease as λ decreases. Furthermore, the central energy density ρ_c required to achieve the maximum mass configuration is always less than that of GR, namely, $\rho_c \lesssim 7\rho_0$ for pure neutron stars and quark stars, and slightly lower for hybrid stars, $\rho_c \lesssim 4.5\rho_0$. The star radii lie in the ranges 8–12 km for pure neutron stars, 8–11 km for quark stars and 9–14 km for hybrid stars.

The mass-radius relation was studied as a function of w for the three types of compact stars and a given a value of the brane tension. As it turns out, the mass-radius curves of neutron stars have a standard behaviour for all values of w , i.e. they bend counterclockwise and the maximum mass is determined by the stability criteria. However, we have found that, for quark and hybrid stars, the curves can bend clockwise for certain negative values of w , reaching the maximum mass at relatively high central densities, $\rho_c \sim 40\rho_0$ (QS) and $\rho_c \sim 45\rho_0$ (HS). In such cases, the maximum allowed mass is determined by the sound speed condition $v_{s,\text{eff}} \leq 1$.

The maximum star mass as a function of λ and w was also studied for the three families of stars. Requiring agreement with observational constraints leads to a lower bound on the brane tension, $\lambda \gtrsim 10^3 \text{ MeV/fm}^3$ for quark and hybrid stars, whereas for pure neutron stars the brane tension can be somewhat lower, $\lambda \gtrsim 6 \times 10^2 \text{ MeV/fm}^3$. For pure neutron and hybrid stars, the dependence of the maximum mass on w are similar, for $w \lesssim -0.5$ and $w \gtrsim -0.2$, the maximum mass remains practically constant with the variation of w and its value is controlled by the value of λ . A remarkable feature in all EOS cases is the fact that the maximum star mass strongly depends on the value of w in a narrow range of this parameter, $-0.3 < w < -0.1$ for neutron and hybrid stars and $-0.4 < w < -0.2$ for quark stars.

Acknowledgments

The work of R.G.F. was partially supported by *Associação do Instituto Superior Técnico para a Investigação e Desenvolvimento* (IST-ID) and *Fundação para a Ciência e a Tecnologia* (FCT) through the projects CERN/FP/123580/2011 and UID/FIS/00777/2013. R.G.F. thanks *Instituto de Cibernética, Matemática y Física* (ICIMAF) in Havana, Cuba, for hospitality.

References

- [1] L. Randall and R. Sundrum, *A Large mass hierarchy from a small extra dimension*, *Phys. Rev. Lett.* **83** (1999) 3370–3373, [[hep-ph/9905221](#)].
- [2] L. Randall and R. Sundrum, *An Alternative to compactification*, *Phys. Rev. Lett.* **83** (1999) 4690–4693, [[hep-th/9906064](#)].
- [3] R. Maartens and K. Koyama, *Brane-World Gravity*, *Living Rev. Rel.* **13** (2010) 5, [[arXiv:1004.3962](#)].
- [4] R. Maartens, D. Wands, B. A. Bassett, and I. Heard, *Chaotic inflation on the brane*, *Phys. Rev.* **D62** (2000) 041301, [[hep-ph/9912464](#)].
- [5] M. C. Bento, R. González Felipe, and N. M. C. Santos, *Sneutrino brane inflation and leptogenesis*, *Phys. Rev.* **D69** (2004) 123513, [[hep-ph/0402276](#)].

- [6] M. C. Bento, R. González Felipe, and N. M. C. Santos, *Gravitational baryogenesis in Gauss-Bonnet braneworld cosmology*, *Phys. Rev.* **D71** (2005) 123517, [[hep-ph/0504113](#)].
- [7] N. Okada and O. Seto, *Thermal leptogenesis in brane world cosmology*, *Phys. Rev.* **D73** (2006) 063505, [[hep-ph/0507279](#)].
- [8] M. C. Bento, R. González Felipe, and N. M. C. Santos, *Aspects of thermal leptogenesis in braneworld cosmology*, *Phys. Rev.* **D73** (2006) 023506, [[hep-ph/0508213](#)].
- [9] D. Psaltis, *Probes and Tests of Strong-Field Gravity with Observations in the Electromagnetic Spectrum*, *Living Rev. Rel.* **11** (2008) 9, [[arXiv:0806.1531](#)].
- [10] C. Germani and R. Maartens, *Stars in the brane world*, *Phys. Rev.* **D64** (2001) 124010, [[hep-th/0107011](#)].
- [11] N. Deruelle, *Stars on branes: The View from the brane*, [gr-qc/0111065](#).
- [12] P. Pani, E. Berti, V. Cardoso, and J. Read, *Compact stars in alternative theories of gravity. Einstein-Dilaton-Gauss-Bonnet gravity*, *Phys. Rev.* **D84** (2011) 104035, [[arXiv:1109.0928](#)].
- [13] J. Ovalle, F. Linares, A. Pasqua, and A. Sotomayor, *The role of exterior Weyl fluids on compact stellar structures in Randall-Sundrum gravity*, *Class. Quant. Grav.* **30** (2013) 175019, [[arXiv:1304.5995](#)].
- [14] L. B. Castro, M. D. Alloy, and D. P. Menezes, *Mass radius relation of compact stars in the braneworld*, *JCAP* **1408** (2014) 047, [[arXiv:1403.1099](#)].
- [15] G. Lugones and J. D. V. Arbañil, *Compact stars on the brane: what could they reveal about extra dimensions*, *Astronomische Nachrichten* **336** (2015) 876.
- [16] K. Schwarzschild, *On the gravitational field of a sphere of incompressible fluid according to Einstein's theory*, *Sitzungsber. Preuss. Akad. Wiss. Berlin (Math. Phys.)* **1916** (1916) 424–434, [[physics/9912033](#)].
- [17] J. M. Lattimer and M. Prakash, *Neutron Star Observations: Prognosis for Equation of State Constraints*, *Phys. Rept.* **442** (2007) 109–165, [[astro-ph/0612440](#)].
- [18] F. Ozel, G. Baym, and T. Guver, *Astrophysical Measurement of the Equation of State of Neutron Star Matter*, *Phys. Rev.* **D82** (2010) 101301, [[arXiv:1002.3153](#)].
- [19] A. W. Steiner, J. M. Lattimer, and E. F. Brown, *The Equation of State from Observed Masses and Radii of Neutron Stars*, *Astrophys. J.* **722** (2010) 33–54, [[arXiv:1005.0811](#)].
- [20] K. Hebeler, J. M. Lattimer, C. J. Pethick, and A. Schwenk, *Constraints on neutron star radii based on chiral effective field theory interactions*, *Phys. Rev. Lett.* **105** (2010) 161102, [[arXiv:1007.1746](#)].
- [21] T. Harko and M. K. Mak, *Vacuum solutions of the gravitational field equations in the brane world model*, *Phys. Rev.* **D69** (2004) 064020, [[gr-qc/0401049](#)].
- [22] A. Chodos, R. L. Jaffe, K. Johnson, C. B. Thorn, and V. F. Weisskopf, *A New Extended Model of Hadrons*, *Phys. Rev.* **D9** (1974) 3471–3495.
- [23] M. Alford, M. Braby, M. W. Paris, and S. Reddy, *Hybrid stars that masquerade as neutron stars*, *Astrophys. J.* **629** (2005) 969–978, [[nucl-th/0411016](#)].
- [24] G. Darrois, “Les équations de la gravitation einsteinienne.” Paris, Gauthier-Villars (Mémoires des sciences mathématiques fasc. 25), 1927.
- [25] W. Israel, *Singular hypersurfaces and thin shells in general relativity*, *Nuovo Cim. Series 10* **B44** (1966) 1.
- [26] C. E. Rhoades, Jr. and R. Ruffini, *Maximum mass of a neutron star*, *Phys. Rev. Lett.* **32** (1974) 324–327.

- [27] N. K. Glendenning, *Limiting rotational period of neutron stars*, *Phys. Rev.* **D46** (1992) 4161–4168.
- [28] S. Koranda, N. Stergioulas, and J. L. Friedman, *Upper limit set by causality on the rotation and mass of uniformly rotating relativistic stars*, *Astrophys. J.* **488** (1997) 799, [[astro-ph/9608179](#)].
- [29] P. Bedaque and A. W. Steiner, *Sound velocity bound and neutron stars*, *Phys. Rev. Lett.* **114** (2015), no. 3 031103, [[arXiv:1408.5116](#)].
- [30] P. Haensel, A. Y. Potekhin, and D. G. Yakovlev, *Neutron stars 1: Equation of state and structure*. New York, USA: Springer, 2007.
- [31] S. Guillot, M. Servillat, N. A. Webb, and R. E. Rutledge, *Measurement of the Radius of Neutron Stars with High S/N Quiescent Low-mass X-ray Binaries in Globular Clusters*, *Astrophys. J.* **772** (2013) 7, [[arXiv:1302.0023](#)].
- [32] J. Antoniadis et al., *A Massive Pulsar in a Compact Relativistic Binary*, *Science* **340** (2013) 6131, [[arXiv:1304.6875](#)].
- [33] R. R. Silbar and S. Reddy, *Neutron stars for undergraduates*, *Am. J. Phys.* **72** (2004) 892–905, [[nucl-th/0309041](#)]. [Erratum: *Am. J. Phys.* 73,286(2005)].
- [34] G. Baym, C. Pethick, and P. Sutherland, *The Ground state of matter at high densities: Equation of state and stellar models*, *Astrophys. J.* **170** (1971) 299–317.
- [35] E. Witten, *Cosmic Separation of Phases*, *Phys. Rev.* **D30** (1984) 272–285.
- [36] C. Alcock, E. Farhi, and A. Olinto, *Strange stars*, *Astrophys. J.* **310** (1986) 261–272.
- [37] **Particle Data Group** Collaboration, K. A. Olive et al., *Review of particle physics*, *Chin. Phys.* **C38** (2014) 090001.
- [38] C. Kettner, F. Weber, M. K. Weigel, and N. K. Glendenning, *Structure and stability of strange and charm stars at finite temperatures*, *Phys. Rev.* **D51** (1995) 1440–1457.